Numerical study of the feasibility of a downslope structure to limit avalanche size during avalanche control activity

Francis Meloche*[1,2,3], Ron Simenhois[4], Don Sharaf[5,6], Ethan Greene[4], Johan Gaume[1,2,3]

[1] *Institute for Geotechnical Engineering, ETH Zürich, CH-8093 Zürich, Switzerland.*
[2] *WSL Institute for Snow and Avalanche Research SLF, CH-7260 Davos Dorf, Switzerland.*
[3] *Climate Change, Extremes, and Natural Hazards in Alpine Regions Research Center CERC, CH-7260 Davos Dorf, Switzerland.*
[4] *Colorado Avalanche Information Center, CAIC, CO, USA.*
[5] *Avalanche Risk Solutions (ARS), Utah, United-States.*
[6] *David Hamre and Associates, LLC, Alaska, United-States*

ABSTRACT: Avalanche defense structures in starting zones are effective, but they are also expensive and visually intrusive; as a result, many highway programs instead rely on active control with explosives. Recent work has shown that crack propagation in the cross-slope direction is slower than in the downslope direction, suggesting that a downslope-oriented structure could arrest propagation and limit release size at a fraction of the cost and visual impact of conventional defense structures. We tested this concept with more than 300 depth-averaged Material Point Method simulations on a simple planar slope, an analytical bowl, and real terrain (Stanley Path, Colorado). We present results considering only buried structures, which locally reduce slab depth and promote tensile fracture of the slab. The slab depth covering the structure was the dominant control, with arrest occurring below 0.15–0.30 m depending on the initial slab density; the structure ratio (height over width) acted as a secondary control, with values of at least 0.5 favoring arrest. The downslope length of the structure should extend to where the slope angle drops below the snow friction angle, and any remaining unprotected gap should not exceed twice the supercritical crack length ($\approx$ 10–15 m at 30°). These results provide a first set of quantitative design guidelines for a new class of downslope-oriented mitigation structures.

KEYWORDS: Crack arrest, avalanche mitigation structures, release size, numerical modeling, depth-averaged Material-Point-Method.

1. INTRODUCTION

Permanent supporting structures installed in avalanche starting zones stabilize the seasonal snowpack and are among the most reliable ways to prevent avalanche release (McClung D. and Schaerer P. 2006; Schweizer, Jamieson, et al. 2003). Traditionally, these structures are placed perpendicular to the fall line, so they carry the creeping and gliding snow cover over their full height. This design works, but the required structure spacing is small and the entire starting zone must be covered; consequently, the cost of installation and maintenance in steep terrain scales with the area to be protected, as does the visual impact on the landscape. For these reasons, many highway avalanche programs rely instead on active mitigation, primarily explosives delivered by hand charges, artillery, or remote avalanche control systems (RACS). Active control is effective, but it exposes personnel to risk, requires repeated operations throughout the season, and does not always prevent large avalanches from reaching the road.

* *Corresponding author address:*
Francis Meloche, ETH Zürich, Switzerland
email: fmeloche@ethz.ch

Dry-snow slab avalanche release is a multiscale mechanical process that begins with damage in a weak layer buried beneath a cohesive slab (McClung D. and Schaerer P. 2006; Schweizer, Jamieson, et al. 2003). Once a crack in the weak layer exceeds a critical length, dynamic crack propagation becomes self-sustained, the slab loses its support, and it starts to move downslope under gravity (Schweizer, Reuter, et al. 2016). Tensile stress then builds up in the slab until it reaches the tensile strength, at which point the slab fractures perpendicular to the weak layer. In some cases, this slab fracture stops propagation and limits release size (Gaume, Chambon, Eckert, Naaim, and Schweizer 2015). Recent work has shown, however, that a slab fracture alone is not sufficient: a significant slow-down of the crack front is also required for arrest to occur (Meloche, Bobillier, et al. 2025; Trottet et al. 2022). This condition is difficult to meet in the downslope direction of a large avalanche, where the crack propagates in the supershear regime at very high speed. In the cross-slope direction, however, crack speeds are considerably lower, making arrest more plausible (Guillet et al. 2023; Simenhois et al. 2023).

This asymmetry is the starting point of the present

https://doi.org/10.15788/1790098836

study. If a crack is easier to stop cross-slope, then a structure oriented *downslope* — that is, parallel to the fall line rather than perpendicular to it — could act as a barrier to lateral propagation and limit the width, and therefore the size, of the release area. Such a structure would not need to support the full downward creeping movement of the snowpack and could therefore be much lighter, cheaper, and less visually intrusive than a conventional snow bridge or snow net. The structure might even be buried, creating a slab depth reduction that still promotes arrest. It could also complement existing RACS installations by confining the release area between two trigger locations.

Here, we evaluate the feasibility of this concept with numerical simulations of dynamic crack propagation. Such a structure could act through two distinct mechanisms: (1) an unburied structure that emerges from the snowpack and physically interrupts the transmission of stress through the slab, and (2) a buried structure that locally reduces the slab depth, thereby promoting a tensile fracture and reducing the driving shear stress available to sustain propagation. Our goal is to determine whether the second concept, a buried structure, is mechanically sound and, if so, to derive quantitative design guidelines — width, height, downslope length, orientation — that can be handed to structural engineers for a subsequent design phase.

2. METHODS

We used a depth-averaged Material Point Method (DAMPM) that resolves shear-driven crack propagation over real terrain (Guillet et al. 2023). The method has already been used to reproduce crack arrest by slab fracture (Meloche, Bobillier, et al. 2025), making it well suited to the question addressed here. The full formulation, validation, and parameterization are described in those two papers, and all configurations and parameter ranges are summarized in Table 1.

Because the model resolves the slab and the weak layer alone, and not the snow beneath them, we cannot represent a 2 m deep snowpack overlying the structure while releasing only its upper 0.5 m. The simulated slab sits directly on the structure and terrain, with no intervening snow to smooth the contact. The structure was therefore modeled as a ridge-like feature with a smooth, Gaussian cross-section rather than a sharp triangular obstacle (Figure 1), since a structure progressively buried by snowfall throughout the season presents a smoothed effective geometry to the slab, regardless of its underlying shape.

Table 1: Simulation configurations and parameter ranges. Slab density and tensile strength are parameterized as a function of the slab depth.

Parameters	Values tested
Terrain	
Planar slope (m)	30 $\times$ 10
Analytical long bowl (m)	80 $\times$ 120
Stanley Path, CO (m)	100 $\times$ 150
Slope angle ψ (°)	35
Snow friction angle ϕ (°)	27
Grid cell size d_x (m)	0.1
Slab	
Initial density ρ_0 (kg m^{-3})	60–100
Slab depth H_{slab} (m)	0.1–0.5
Density ρ (kg m^{-3})	$f(H_{slab})$
Tensile strength σ_t (kPa)	$f(H_{slab})$
Weak layer	
Shear strength τ_p (kPa)	1 (or infinite)
Structure	
Width W_{wall} (m)	0.15–15
Height H_{wall} (m)	0.1–3
Ratio H_{wall}/W_{wall} (–)	0.1–0.8
Downslope length (m)	40–120
Orientation (° from x-axis)	-30–20
Simulation	
Total number of runs (–)	$>$300
Total data volume (Tb)	$>$18

2.1. Slab parameterization

The mechanism of interest is the local reduction of slab depth over the buried structure, so the mechanical properties of the slab must respond to that reduction. We therefore parameterized both slab density and slab tensile strength as functions of slab depth (Figure 1a), using the cold-laboratory measurements of Sigrist (2006) and the empirical power-law fit of McClung (2009). The initial density ρ_0 of this parameterization was varied between 60 and 100 kg m^{-3}, with lower values representing calm storm snow or a continental snowpack and higher values representing wind slab or a maritime snowpack.

2.2. Terrain configurations

Three terrain configurations were used (Figure 1). The first is a simple planar slope (30 $\times$ 10 m) in which only cross-slope propagation is simulated; it is computationally inexpensive and was used for the broad sensitivity analysis. The second is an analytical long bowl (80 $\times$ 120 m) that avoids boundary effects and allows downslope and cross-slope propagation to develop simultaneously at steady state (Figure 1b). The third is the Stanley Path above US Highway 40 in Colorado (100 $\times$ 150 m), where two GazEx remote avalanche

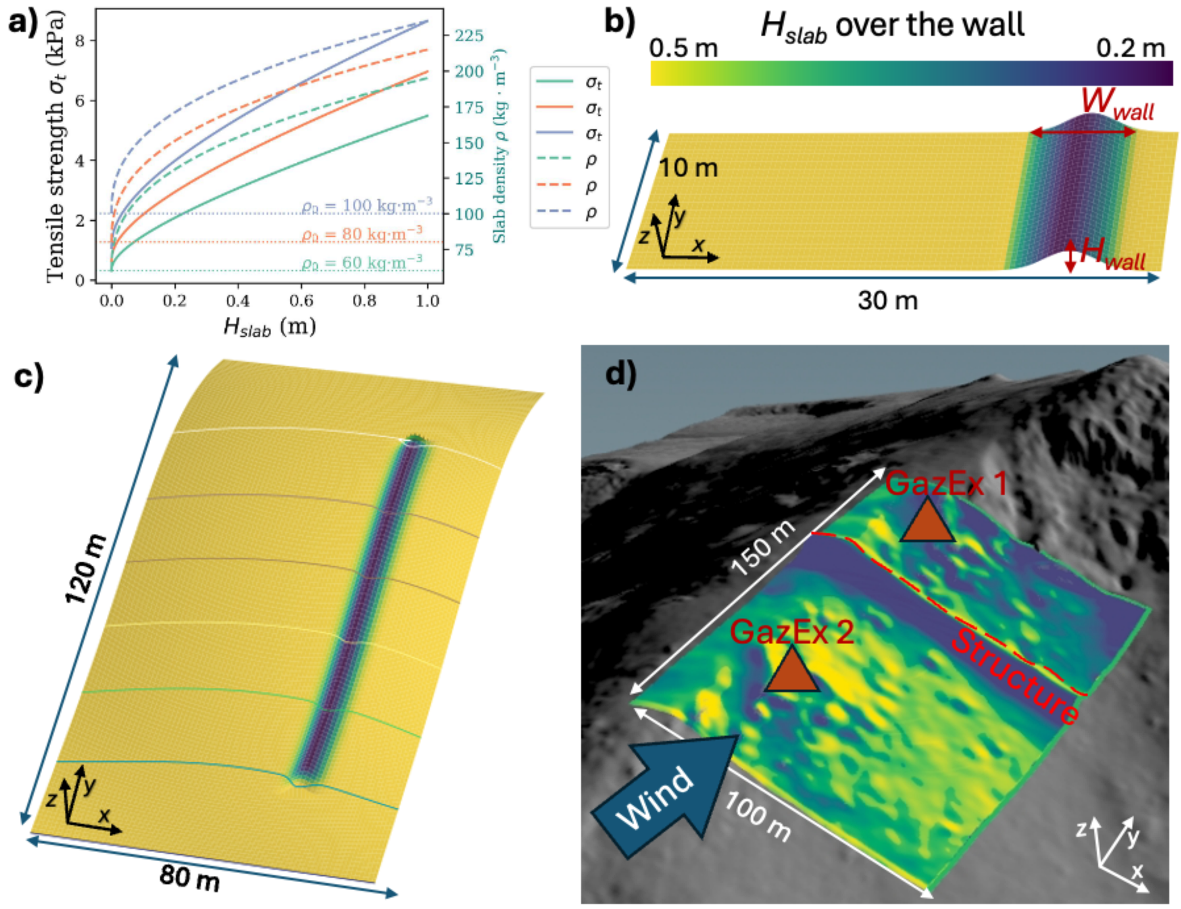

Figure 1: Simulation geometries and slab depth parameterization. a) Slab density and tensile strength as a function of slab depth, for three initial densities ρ_0, after Sigrist (2006) and McClung (2009). b) Long-bowl simulation with the Gaussian ridge structure. c) Complex terrain simulation on the Stanley Path, Colorado, with the structure placed between the two GazEx positions. The colormap for slab depth is defined in a).

control systems are installed in the starting zone and where the proposed structure would be placed between them (Figure 1c). To obtain a realistic spatial distribution of slab depth on this terrain, we applied the Winstral terrain-based parameterization of wind redistribution (Winstral et al. 2002) with a wind direction producing a cross-loaded slope, a scenario that local forecasters associate with the largest avalanches. The resulting slab depth varied from about 0.1 to 0.5 m across the slope.

2.3. Characteristic lengths

Two characteristic lengths are used throughout to interpret the results. The first is the characteristic elastic length Λ of the slab-weak layer system, which measures how far ahead of the crack tip the disturbance is felt through elastic redistribution in the slab (Chiaia et al. 2008; Gaume, Chambon, Eckert, and Naaim 2013). The second is the supercritical crack length a_{sc}, the damaged weak layer length required to sustain shear-driven propagation (Gaume, Chambon, Eckert, and Naaim 2013; Trottet et al. 2022). Because a_{sc} describes only the portion of the slab in tension above the crack, the total damaged length required in an open slope is approximately $2a_{sc}$, which accounts for the compressive zone below (Chiaia et al. 2008; Gaume, Chambon, Eckert, and Naaim 2013). For a 30° slope and the snow properties used here, $2a_{sc}$ is of the order of 10–15 m.

3. RESULTS

3.1. Slab depth and structure ratio

Using the planar slope simulations, a partial dependence analysis over the six tested parameters — slab depth over the wall H_{slab}, wall width W_{wall}, wall height H_{wall}, slab depth reduction length L_{reduc}, cross-loading asymmetry S_{asym}, and initial density ρ_0 — shows that H_{slab} and ρ_0 dominate

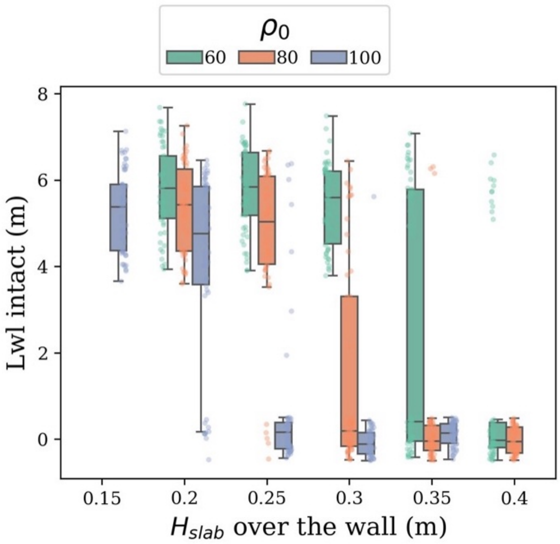

Figure 2: Effectiveness of a buried downslope structure in arresting weak layer crack propagation. a) Intact weak layer length $L_{wl,intact}$ versus slab depth above the structure H_{slab} for three initial slab densities ρ_0; high values indicate arrest and $L_{wl,intact} = 0$ indicates full propagation.

the distinction between arrest and propagation, whereas the remaining parameters explain only residual variability.

Figure 2 shows the intact weak layer length as a function of the slab depth covering the structure for three initial densities. A clear, density-dependent threshold emerges: propagation with denser slabs crosses the structure at shallower burial depths. The threshold slab depth varies from about 0.30 m for $\rho_0 = 60$ kg m^{-3} down to about 0.15 m for $\rho_0 = 100$ kg m^{-3}. In other words, thicker and stronger slabs — above roughly 150 kg m^{-3} and 4 kPa of tensile strength at the structure — will propagate across it regardless of the geometry.

The long-bowl simulations reproduce this threshold at 0.20–0.25 m for $\rho_0 = 80$ kg m^{-3}, in agreement with the planar slope results, and reveal the role of the secondary variable. At the threshold, and only there, the structure ratio H_{wall}/W_{wall} becomes decisive: arrest occurred exclusively for ratios of 0.5 or above, which produce a local slope steep enough at the structure to hinder the crack. Away from the threshold, the ratio has little influence. The distance between the trigger and the structure, varied from the far edge of the slope to approximately 5 m, had a negligible effect within the tested range.

3.2. Downslope length and terrain

A structure that stops crack propagation across most of the slope but leaves an unprotected gap near the top is of little use. At the same time, a shorter structure is cheaper to build, so the minimum effective length is of practical interest. Our long-bowl simulations with structure lengths between 40 and 120 m show that the crack bypasses the barrier through this upper gap once the gap exceeds a threshold length (Figure 3). For $H_{slab} = 0.3$ m, propagation bypasses the structure regardless of the tested structure length. For thinner slabs, arrest was obtained with a 65 m structure at $H_{slab} = 0.2$ m and with a 70 m structure at $H_{slab} = 0.25$ m, corresponding to remaining unprotected lengths of 15 m and 12 m, respectively.

These two values are close to $2a_{sc}$, which is 10–15 m for the slope angles and snow properties simulated here. They also correspond to the point where the slope angle drops below the snow friction angle of 27°, so that gravitational shear stress can no longer sustain shear-driven propagation. The gap criterion and the friction-angle criterion therefore give the same answer here, which is convenient for design: both indicate that the structure should extend to where the slope flattens below ϕ, and that any remaining gap should stay below $2a_{sc}$.

3.3. Stanley Path case study

The Stanley Path simulations, run with the wind-driven slab depth distribution described above, reproduce the thresholds found on the idealized terrain. Almost all simulations with a minimum H_{slab} of 0.15 m arrested at the barrier, both through slab fracture at the thinned zone and through the reduction in driving shear stress caused by the lower slab weight and locally steeper terrain. At 0.2 m, a slab tensile fracture still occurred at the structure, but the shear stress remained sufficient to sustain propagation across it in most cases.

The simulations that did arrest at 0.2 m are those combining a structure ratio at or above 0.5 with an orientation greater than 10° from the x-axis (Figure 4). The single arrest obtained with a thicker slab had a ratio of 0.8 and an orientation of 20°. That configuration is, however, both very close to the GazEx trigger location, which may have influenced the result, and close to a cross-slope arrangement resembling a conventional snow fence, which defeats the purpose of a downslope structure. Orientations between 0° and 10° therefore appear to be the practical optimum, requiring

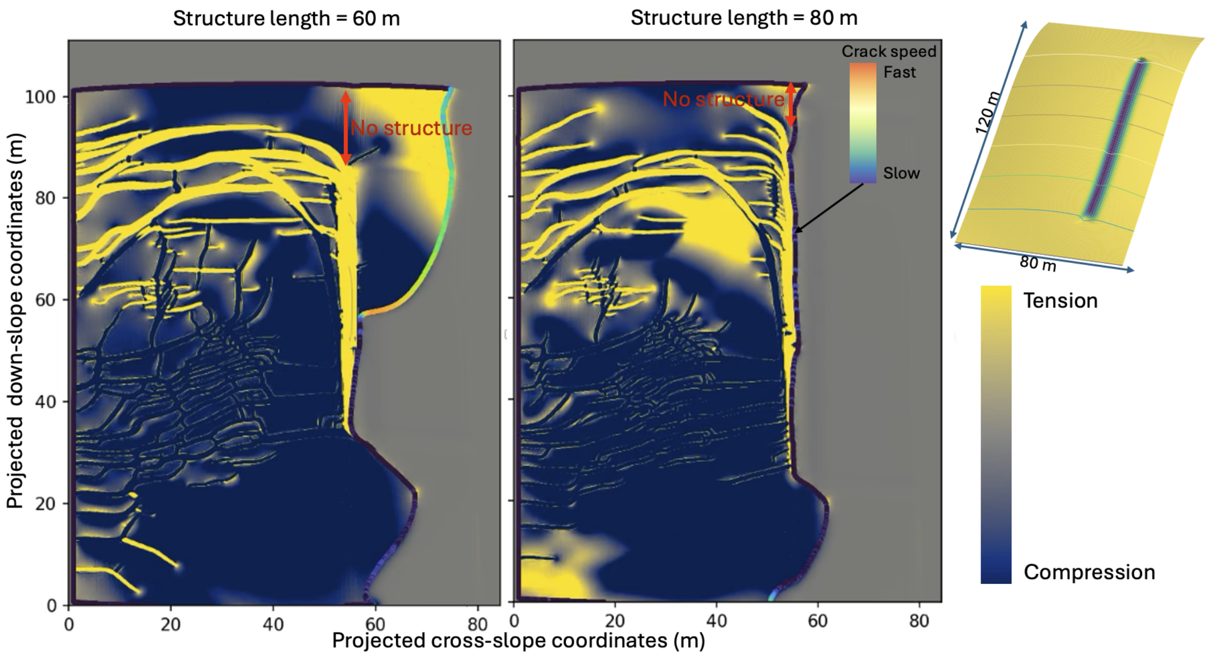

Figure 3: Influence of structure length on crack arrest. a) Intact weak layer area versus structure length for three slab depths H_{slab}. A length threshold of 65–70 m is required to arrest cracks in thinner slabs (0.20–0.25 m), while thicker slabs (0.3 m) propagate regardless of structure length. b) Downslope profile of slope angle relative to the snow friction angle (dashed). Effective arrest depends on minimizing the unprotected gap of steep terrain above the structure; when this gap exceeds $2a_{sc}$ ($\approx$ 10–15 m), the crack gains enough energy to propagate around the structure.

$H_{slab} \leq 0.2$ m, while orientations between $-10°$ and $-20°$ require a thinner cover of about 0.15 m.

4. DISCUSSION

Taken together, these simulations indicate that a buried downslope-oriented structure can arrest cross-slope crack propagation, and they identify which dimensions matter most. The hierarchy is consistent across all three terrain configurations: the slab depth covering the structure is the primary control, the structure ratio is a secondary control that becomes decisive only near the threshold slab depth, and the distance from the trigger is essentially irrelevant within the ranges we tested.

The dominant role of slab depth covering the structure leads to a clear conceptual requirement: the structure should be designed to emerge from the snowpack as much as possible, with a height comparable to the average snow depth at the potential site. Snow depth maps or historical snow depth records in the candidate release area are therefore a prerequisite for dimensioning. Regular avalanche control should also be maintained, since the tolerance is small — as little as 0.3 m of accumulated slab above the structure can be enough to allow propagation, and less than that in denser snow. However, this value of accumulated slab could be higher in cases where the structure also promote the weak layer discontinuity, as this case is very probable considering the heterogeneous nature of snow. This is a demanding requirement and represents the main practical limitation of the concept.

Our results also indicate that the downslope extent of the structure should run from the ridge down to where the slope angle falls below the snow friction angle, because shear-driven propagation cannot be sustained below that angle. Where terrain or logistics prevent this, the remaining unprotected gap should not exceed $2a_{sc}$, typically 10–15 m on a 30° slope. Both the structure length threshold in the long-bowl simulations and the spacing threshold for discontinued structures converge on this length, suggesting that a_{sc} — computable from snow properties and slope angle — can serve as a planning quantity, estimated in advance from a DEM together with snow cover model output.

We had also hoped that the structure might introduce a delay long enough to split one large avalanche into two smaller ones. The measured delays were 0.3–0.5 s in both the long-bowl and Stanley Path configurations, which are far too

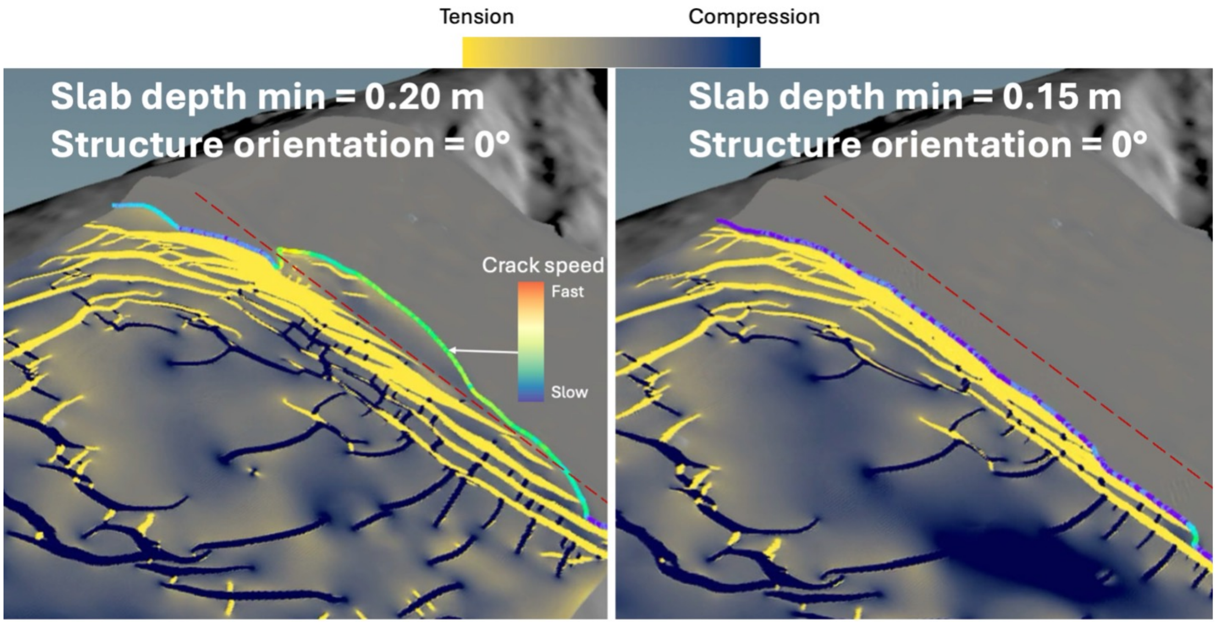

Figure 4: Stanley Path case study. a) Two simulations with different minimum slab depths over the structure at 0° orientation; the blue-yellow colormap shows tensile and compressive stress in the slab, and the colored outline the crack front and crack speed. b) Sensitivity analysis: intact weak layer area versus slab depth, with symbols indicating the structure ratio H_{wall}/W_{wall} and colors the structure orientation relative to the x-axis. Slab depth is the primary control; at 0.2 m, arrest additionally requires a ratio $\geq$ 0.5 and an orientation above 10°.

small for that. Larger delays are conceivable if, instead of arresting, the crack drops from the shear-based regime (roughly 80–100 m s^{-1} cross-slope in mode III) to the collapse-based anticrack regime (roughly 40 m s^{-1}), which would result in delays on the order of 1 s. Our depth-averaged model by construction cannot reproduce that transition, so we could not test it; however, even a 1 s delay remains modest, and we would not recommend designing a structure around this mechanism.

Several limitations should be kept in mind. First, the model reproduces shear-based propagation only. This is appropriate for the large, fast avalanches that motivate the study, but it means that where we report an arrest, the real outcome could instead be a transition to slower anticrack propagation across the structure (Trottet et al. 2022). We are currently conducting full three-dimensional simulations capable of resolving the transition between the anticrack sub-Rayleigh regime and supershear propagation. These will indicate whether the arrest thresholds reported here still hold once this transition is captured. Second, the weak layer was spatially homogeneous. Real weak layers are heterogeneous, and heterogeneity is known to favor arrest (Gaume, Chambon, Eckert, and Naaim 2013; Meloche, Gauthier, et al. 2023; Reuter et al. 2016); the slab depth thresholds we report are therefore likely conservative, and thicker cover may still produce arrest in the field. Third, the model resolves only the slab, the weak layer, and the terrain beneath, so we could not simulate the burial process itself or the modification of the local wind field by the structure. That modification is not a detail: a structure will generate its own erosion and deposition patterns, increasing both burial depth and effective width, and thereby lowering the structure ratio our results require to stay above 0.5. Three-dimensional wind-field models now make this tractable around buildings (Hames et al. 2025) and alpine solar installations (Frischholz et al. 2026), and applying them to this geometry is an obvious next step.

Finally, the mechanism of arrest itself is not fully understood. We know from Meloche, Bobillier, et al. (2025) that arrest requires an interplay between a relative decrease in crack speed — from higher weak layer strength or lower slope angle — and slab fracture, but the magnitude of the slow-down required to convert a slab fracture into an arrest has not been quantified. Therefore, general rules covering snow properties and structural dimensions outside our tested parameter space cannot be derived with confidence.

5. CONCLUSION

We evaluated, through more than 300 depth-averaged MPM simulations on planar, analytical, and real terrain, whether a downslope-oriented vertical structure can arrest weak layer crack propagation and limit avalanche release size. The concept is mechanically sound, and the governing dimensions are now quantified. Arrest by a buried structure is controlled primarily by the slab depth covering it, with thresholds between 0.15 and 0.30 m depending on initial density, and secondarily by a structure height-to-width ratio of at least 0.5. The downslope extent should reach the point where the slope angle drops below the snow friction angle, with any remaining unprotected gap kept under twice the supershear critical crack length, and the structure should be oriented within 10° of the fall line to remain distinct from a conventional cross-slope fence.

Delays introduced by the structure were too short to split a release into two events, so arrest, not delay, is the mechanism to design for. The next phase should therefore address the structural engineering problem this study leaves open: a design that emerges from the snowpack, resists wind loading and multi-season snow stresses, and maintains a height-to-width ratio above 0.5 once buried, coupled with three-dimensional wind-field modeling of snow accumulation around it. A prototype deployment at the Stanley Path, between the existing GazEx installations, would allow these predictions to be tested directly.

ACKNOWLEDGEMENTS

This work was funded by the Transportation Avalanche Research Pool (TARP), and the full report is available at `https://rosap.ntl.bts.gov/view/dot/92468`. We also thank David Hamre for his guidance throughout the project.

REFERENCES

Chiaia, B. M., Cornetti, P., and Frigo, B. (2008). Triggering of dry snow slab avalanches: stress versus fracture mechanical approach. In: Cold Regions Science and Technology 53.2, pp. 170–178. ISSN: 0165232X. https://doi.org/10.1016/j.coldregions.2007.08.003.

Frischholz, Y., Hames, O., and Lehning, M. (Jan. 2026). Optimizing snow distribution in alpine PV systems: CFD-based design guidelines for power plant layout. In: Cold Regions Science and Technology 241, p. 104654. ISSN: 0165232X. https://doi.org/10.1016/j.coldregions.2025.104654.

Gaume, J., Chambon, G., Eckert, N., Naaim, M., and Schweizer, J. (2015). Influence of weak layer heterogeneity and slab properties on slab tensile failure propensity and avalanche release area. In: Cryosphere 9.2, pp. 795–804. ISSN: 19940424. https://doi.org/10.5194/tc-9-795-2015.

Gaume, J., Chambon, G., Eckert, N., and Naaim, M. (2013). Influence of weak-layer heterogeneity on snow slab avalanche release: Application to the evaluation of avalanche release depths. In: Journal of Glaciology 59.215, pp. 423–437. ISSN: 00221430. https://doi.org/10.3189/2013JoG12J161.

Guillet, L., Blatny, L., Trottet, B., Steffen, D., and Gaume, J. (July 2023). A Depth-Averaged Material Point Method for Shallow Landslides: Applications to Snow Slab Avalanche Release. In: Journal of Geophysical Research: Earth Surface, pp. 1–28. ISSN: 2169-9011. https://doi.org/10.1029/2023JF007092.

Hames, O., Jafari, M., Köhler, P., Haas, C., and Lehning, M. (Mar. 2025). Governing Processes of Structure-Borne Snowdrifts: A Case Study at Neumayer Station III. In: Journal of Geophysical Research: Earth Surface 130.3. ISSN: 2169-9003. https://doi.org/10.1029/2024JF008180.

McClung, D. M. (Mar. 2009). Dimensions of dry snow slab avalanches from field measurements. In: Journal of Geophysical Research: Earth Surface 114.1. ISSN: 21699011. https://doi.org/10.1029/2007JF000941.

McClung D. and Schaerer P. (2006). The Avalanche Hanbook. The Mountaineers Books.

Meloche, F., Bobillier, G., Guillet, L., Gauthier, F., Langlois, A., and Gaume, J. (Dec. 2025). Modeling Crack Arrest in Snow Slab Avalanches—Toward Estimating Avalanche Release Sizes. In: Journal of Geophysical Research: Earth Surface 130.12. ISSN: 2169-9003. https://doi.org/10.1029/2025JF008470.

Meloche, F., Gauthier, F., and Langlois, A. (2023). Snow mechanical properties variability at the slope scale, implication for snow mechanical modeling. In: Preprint EGUsphere. https://doi.org/https://doi.org/10.5194/egusphere-2023-1586.

Reuter, B., Richter, B., and Schweizer, J. (2016). Snow instability patterns at the scale of a small basin. In: Journal of Geophysical Research: Earth Surface 121.2, pp. 257–282. ISSN: 21699011. https://doi.org/10.1002/2015JF003700.

Schweizer, J., Reuter, B., Herwijnen, A. van, and Gaume, J. (2016). “Avalanche Release 101”. In: International Snow Science Workshop, Breckenridge, Colorado. Breckenridge, pp. 1–11.

Schweizer, J., Jamieson, J. B., and Schneebeli, M. (2003). Snow avalanche formation. In: Reviews of Geophysics 41.4, pp. 3–5. ISSN: 87551209. https://doi.org/10.1029/2002RG000123.

Sigrist, C. (2006). “Measurement of fracture mechanical properties of snow and application to dry snow slab avalanche release”. PhD thesis. Zürich: ETH Zürich. https://doi.org/10.3929/ETHZ-A-005282374.

Simenhois, R., Birkeland, K. W., Gaume, J., Van Herwijnen, A., Bergfeld, B., Trottet, B., and Greene, E. (2023). Using video detection of snow surface movements to estimate weak layer crack propagation speeds. In: Annals of glaciology, pp. 1–11. https://doi.org/10.1017/aog.2023.36.

Trottet, B., Simenhois, R., Bobillier, G., Bergfeld, B., Herwijnen, A. van, Jiang, C., and Gaume, J. (July 2022). Transition from sub-Rayleigh anticrack to supershear crack propagation in snow avalanches. In: Nature Physics 18.9, pp. 1094–1098. ISSN: 1745-2481. https://doi.org/10.1038/s41567-022-01662-4.

Winstral, A., Elder, K., and Davis, R. E. (2002). Spatial snow modeling of wind-redistributed snow using terrain-based parameters. In: Journal of Hydrometeorology 3.5, pp. 524–538. ISSN: 1525755X. https://doi.org/10.1175/1525-7541(2002)003<0524:SSMOWR>2.0.CO;2.